



CHORUS

This is the accepted manuscript made available via CHORUS. The article has been published as:

Probing fission fragment angular momenta by photon measurements

Jørgen Randrup, Thomas Døssing, and Ramona Vogt

Phys. Rev. C **106**, 014609 — Published 18 July 2022

DOI: [10.1103/PhysRevC.106.014609](https://doi.org/10.1103/PhysRevC.106.014609)

Probing fission fragment angular momenta by photon measurements

Jørgen Randrup¹, Thomas Døssing² and Ramona Vogt^{3,4}

¹*Nuclear Science Division,
Lawrence Berkeley National Laboratory,
Berkeley, CA 94720, USA*

²*Niels Bohr Institute, Copenhagen Denmark*

³*Physics Division, Lawrence Livermore National Laboratory,
Livermore, CA 94551, USA*

⁴*Physics Department, University of California,
Davis, CA 95616, USA*

(Dated: July 6, 2022)

We discuss how the measurement of photon angular correlations can reveal information about the orientation of the fission fragment angular momenta. Photons from identified stretched E2 collective transitions in even-even fission product nuclei are particularly suitable because they do not affect the orientation of the nuclear spin. Their angular distribution relative to the direction of a fission fragment may reveal the orientation of the fragment spins relative to the fission axis. A novel means of probing the correlated fission fragment spins is the distribution of the opening angle between E2 photons from even-even partner fragments which reveals the mutual correlation of the fragment spins, if the photon helicities can be determined, demonstrating the potential power of helicity measurements in fission.

I. INTRODUCTION

The interest in the generation of angular momentum in fission fragments and its observational consequences is currently intensifying and quite a number of papers on this topic have appeared recently, both theoretical and experimental [1–12].

Low-energy fission leads to fragments that typically carry about half a dozen units of angular momentum. The average spin magnitude exhibits a sawtooth-like dependence on the fragment mass number [2, 4, 13] as well as a dependence on the total fragment kinetic energy [2, 13]. Furthermore, recent measurements of photons from identified rotational transitions in certain product nuclei led Wilson *et al.* to conclude that the magnitudes of the two fragment spins are largely uncorrelated [4], though the associated correlation coefficient has yet to be determined. Regarding the fragment spin directions, it has long been known, from measurements of the photon angular distribution relative to the direction of the fragment motion [14, 15], that the angular momenta of the primary fragments tend to be perpendicular to the fission axis, but the large error bars associated with those pioneering measurements preclude a precise determination of the spin direction. Finally, nothing is known experimentally about the directional correlation between the two partner fragment spins.

The main purpose of this paper is to show how suitable photon measurements may provide information about the directions of the fragment angular momenta, either with respect to the fission axis or relative to one another, and to discuss how such measurements may help to determine the relative presence of the various dinuclear rotational modes at the time of scission.

In order to establish the conceptual framework for our study, we first, in Sect. II, discuss the angular-momentum

bearing modes in the dinuclear complex as scission is approached. Subsequently, in Sect. III, we briefly recall those elements of the Nucleon-Exchange Transport model that are relevant for the generation of fission fragment angular momentum, including the relaxation times associated with the various normal rotational modes. Then, in Sect. IV, we briefly describe recent improvements in the treatment of the photon cascade in the FREYA fission simulation code. Section V discusses how the angular distribution of the E2 photons reveals the orientation of the the fragment spins relative to the fission axis and Sect. VI discusses the use of the opening angle between helicity-tagged E2 photons from partner fragments to probe the relative orientation of the fragment spins. Finally, Sect. VII presents our concluding remarks.

II. FRAGMENT ANGULAR MOMENTA

We review here a convenient framework for discussing the fission fragment angular momenta.

As the fissioning system approaches scission, it progressively develops a binary character and eventually it consists of two nascent fragments in close proximity. While these may be significantly distorted (relative to their individual equilibrium shapes) and still be subject to the inter-nuclear (proximity) force, their nucleon numbers, (Z_L, N_L) and (Z_H, N_H) , are now frozen in.

The two proto-fragments are generally in relative motion and their angular momentum is $\mathbf{L} = \mathbf{R} \times \mathbf{P}$. Here $\mathbf{R} \equiv \mathbf{R}_L - \mathbf{R}_H$ is the position of the light proto-fragment relative to the heavy one; the direction of \mathbf{R} at the time of scission is referred to as the fission axis. Furthermore, the relative momentum is given by $\mathbf{P} = \mu(\mathbf{V}_L - \mathbf{V}_H)$ with \mathbf{V}_i being the velocity of fragment i and $\mu \approx mA_L A_H / (A_L + A_H)$ denoting the reduced

mass of the fragments. The individual proto-fragments also generally have angular momenta, \mathbf{S}_L and \mathbf{S}_H , so the total angular momentum of the binary complex is $\mathbf{S}_0 = \mathbf{S}_L + \mathbf{S}_H + \mathbf{L}$. Because the system is isolated, both its total linear momentum, $\mathbf{P}_0 \approx m(A_L \mathbf{V}_L + A_H \mathbf{V}_H)$, and its total angular momentum, \mathbf{S}_0 , are conserved.

There is currently considerable interest in both the magnitudes and the directions of the fragment spins. A convenient reference for these discussions can be obtained by bringing the angular-momentum bearing modes in the dinuclear complex on normal form [16–18],

$$E_0^{\text{rot}} = \frac{S_L^2}{2\mathcal{I}_L} + \frac{S_H^2}{2\mathcal{I}_H} + \frac{(\mathbf{S}_0 - \mathbf{S}_L - \mathbf{S}_H)^2}{2\mathcal{I}_R} \quad (1)$$

$$= \frac{S_0^2}{2\mathcal{I}_0} + \frac{s_{\text{wrig}}^2}{2\mathcal{I}_{\text{wrig}}} + \frac{s_{\text{bend}}^2}{2\mathcal{I}_{\text{bend}}} + \frac{s_{\text{twst}}^2}{2\mathcal{I}_{\text{twst}}} + \frac{s_{\text{tilt}}^2}{2\mathcal{I}_{\text{tilt}}}. \quad (2)$$

Here \mathcal{I}_L and \mathcal{I}_H are the moments of inertia of the individual fragments, $\mathcal{I}_R = \mu R^2$ is the moment of inertia for the orbital motion, and $\mathcal{I}_0 = \mathcal{I}_L + \mathcal{I}_H + \mathcal{I}_R$ is the total moment of inertia. The various normal modes were imaginatively named by Nix and Swiatecki [16] and we now discuss them in turn.

Overall rotation: Generally, the fissioning system has an overall angular momentum \mathbf{S}_0 . The lowest rotational energy occurs when none of the normal modes are agitated and the combined system rotates rigidly. The various normal modes, which carry no net angular momentum, then provide fluctuating contributions on top of this rigid rotation. Typically, in low-energy fission, these contributions are dominant [8] while the rigid rotation is negligible. In the present study, which is primarily exploratory, we focus on $^{252}\text{Cf}(\text{sf})$ for which the total angular momentum is strictly zero, $S_0 = 0$. The results are expected to remain essentially unchanged for other common fission cases, such as $^{235}\text{U}(n_{\text{th}},\text{f})$ or $^{239}\text{Pu}(n_{\text{th}},\text{f})$.

Wriggling: The spin contributions from wriggling are perpendicular to the fission axis \mathbf{R} and mutually parallel,

$$\delta\mathbf{S}_{L,H}^{\text{wrig}} = \frac{\mathcal{I}_{L,H}}{\mathcal{I}_L + \mathcal{I}_H} \mathbf{s}_{\text{wrig}}, \quad \delta\mathbf{L}^{\text{wrig}} = -\mathbf{s}_{\text{wrig}}, \quad (3)$$

with $\mathcal{I}_{\text{wrig}} = (\mathcal{I}_L + \mathcal{I}_H)\mathcal{I}_R/\mathcal{I}_0$. The associated change of \mathbf{L} is mandated by angular momentum conservation which also reduces the moment of inertia by the factor $\mathcal{I}_R/\mathcal{I}_0$. Because the space perpendicular to \mathbf{R} is two-dimensional, there are two independent and degenerate wriggling modes.

Bending: The contributions to the fragment spins from bending are also perpendicular to the fission axis but perfectly opposite,

$$\delta\mathbf{S}_L^{\text{bend}} = \mathbf{s}_{\text{bend}}, \quad \delta\mathbf{S}_H^{\text{bend}} = -\mathbf{s}_{\text{bend}}, \quad \delta\mathbf{L}^{\text{bend}} = \mathbf{0}, \quad (4)$$

with $\mathcal{I}_{\text{bend}} = \mathcal{I}_L\mathcal{I}_R/(\mathcal{I}_L + \mathcal{I}_R)$. Because the contributions to the fragment spins are exactly opposite, bending has no effect on \mathbf{L} . As is the case for wriggling, there are two independent and degenerate bending modes.

Twisting: Twisting is similar to bending but directed along the fission axis, $\mathbf{s}_{\text{twst}} = s_{\text{twst}}\hat{\mathbf{R}}$,

$$\delta\mathbf{S}_L^{\text{twst}} = \mathbf{s}_{\text{twst}}, \quad \delta\mathbf{S}_H^{\text{twst}} = -\mathbf{s}_{\text{twst}}, \quad \delta\mathbf{L}^{\text{twst}} = \mathbf{0}, \quad (5)$$

with $\mathcal{I}_{\text{twst}} = \mathcal{I}_{\text{bend}}$.

Tilting: In tilting the two fragment spin contributions are parallel along the fission axis, $\mathbf{s}_{\text{tilt}} = s_{\text{tilt}}\hat{\mathbf{R}}$,

$$\delta\mathbf{S}_i^{\text{tilt}} = \frac{\mathcal{I}_i}{\mathcal{I}_{\text{tilt}}} \mathbf{s}_{\text{tilt}}, \quad \delta\mathbf{L}^{\text{tilt}} = -\mathbf{s}_{\text{tilt}}, \quad (6)$$

with $\mathcal{I}_{\text{tilt}} = \mathcal{I}_L + \mathcal{I}_H$. Because the system is isolated, this mode cannot be excited directly and appears only as a result of the tilting of the orbital plane of motion in response to wriggling recoils perpendicular to \mathbf{L} . The characteristic time scale for tilting is therefore very long [18] and we may disregard this mode in the present study.

The above discussion shows how the angular momenta of the emerging fragments are built up of contributions from the various normal dinuclear rotational modes. The models for fission fragment spins then differ in the degree to which those modes are populated, which is reflective of the mechanisms invoked. The purpose of the present paper is to demonstrate how some light may be shed on this issue by suitable photon measurements.

A further useful reference is provided by the thermal limit in which all the modes are populated in accordance with the appropriate statistical distributions, as first considered by Motetto [17]. Then the distribution of the spin fluctuations associated with mode m has the form $P_m(s_m) \sim \exp(-s_m^2/2\mathcal{I}_m T)$ and the corresponding spin variance is $\langle s_m^2 \rangle_T = \mathcal{I}_m T$, where T is the effective temperature of the dinuclear complex. Whether this limit is realized in fission depends on the characteristic time scales for the agitation of those modes.

III. ANGULAR MOMENTUM DYNAMICS

In the preceding section, we have discussed the various angular-momentum bearing modes in the dinuclear system. For each of the normal modes there is a relaxation time, t_m , which gives the time scale for the mode to acquire its equilibrium form. If t_m is significantly shorter than the time associated with the descent of the barrier towards scission, it can be expected that the mode will have its equilibrium form at the time scission occurs, but otherwise the mode is not fully adjusted at scission. It is therefore important to investigate these time scales.

Our expectations regarding the dinuclear rotational time scales may be guided by the Nucleon Exchange Transport model [19, 20]. Although it was developed primarily for understanding the dynamical evolution of damped nuclear reactions [21, 22], the basic physics applies equally well for the late stages of fission when the system acquires a binary character.

The relaxation time for the mode m is given by $t_m = \mathcal{I}_m/M_m$, where \mathcal{I}_m is the moment of inertia for the mode

(see above) and M_m is its mobility coefficient. Expressions for the mobility coefficients were derived in [18] based on the Nucleon Exchange Transport model presented in [20],

$$M_{\text{wrig}} = m\mathcal{N}R^2, \quad (7)$$

$$M_{\text{bend}} = m\mathcal{N} \left[\left(\frac{\mathcal{I}_H R_L - \mathcal{I}_L R_H}{\mathcal{I}_L + \mathcal{I}_H} \right)^2 + c_{\text{ave}}^2 \right], \quad (8)$$

$$M_{\text{twst}} = m\mathcal{N}c_{\text{ave}}^2. \quad (9)$$

Here the rate of nucleon transfers from one fragment to the other is given by $\mathcal{N} \approx \frac{1}{4}\rho\bar{v}\pi c^2$ [23] where ρ is the standard nucleon density, $\bar{v} = \frac{3}{4}v_F$ is the mean nucleon speed, and c is the neck radius. Furthermore, $c_{\text{ave}}^2 = \frac{1}{2}c^2$ is the average value of c^2 . M_{twst} is an order of magnitude smaller than M_{wrig} because $c^2 \ll R^2$, so $t_{\text{twst}} \gg t_{\text{wrig}}$. The first term in M_{bend} vanishes for symmetric divisions, giving $M_{\text{bend}} = M_{\text{twst}}$, but M_{bend} is significantly larger than M_{twst} for typical mass divisions (and small neck radii). These relaxation times are shown in Fig. 1 as functions of c , using $R = R_L + R_H + d$ with $d = 4$ fm.

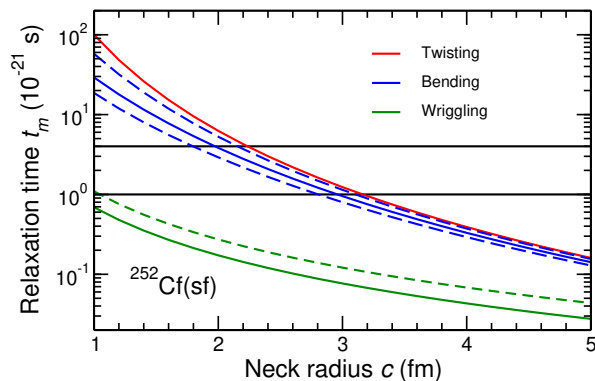


FIG. 1: The calculated relaxation times t_m for wriggling (bottom curve, green), bending (middle three curves, blue), and twisting (top curve, red), shown as functions of the neck radius c for a tip separation of $d = 4$ fm. For wriggling is also shown the result for touching spheres, $d = 0$ (dashed green). For bending, the solid curve is for the mass division 108:144 (the most probable), while the dashed curves are for 100:152 (lower) and 118:134 (upper) which are each half as probable. Also shown are $t_{\text{fiss}}=1$ and $t_{\text{fiss}}=4$ zs (horizontal lines).

In order to put the calculated relaxation times into perspective, they should be compared with t_{fiss} , the time it takes the fissioning system to evolve from the first appearance of a dinuclear geometry to the rupture of the neck. This quantity is difficult to measure experimentally and it is not well known [24, 25]. The discussion below assumes that t_{fiss} is in the range of one to several zeptoseconds (1 zs = 10^{-21} s).

The calculated t_{wrig} stays well below the expected range of t_{fiss} and one should therefore expect that the wriggling mode maintains full equilibrium until the time of scission, which is expected to occur for $c \approx 2$ fm.

By contrast, t_{twst} is likely similar to or longer than t_{fiss} , so the twisting mode will adjust only slowly as scission is approached. Therefore, for spontaneous fission, where the rotational modes are probably not agitated much as the system emerges from the tunneling, it may not be possible to build up very much twisting before scission occurs. The situation is more complicated for induced fission. For thermal neutron energies the local excitation energy in the barrier region is small and even though the system spends a fairly long time there, the low local temperature will limit the degree of agitation of the rotational modes and, consequently, it may not be possible for the twisting mode to adjust to the ever-increasing temperature as scission is approached. But, as the neutron energy is raised, the local temperature in the saddle region increases correspondingly and the twisting mode is more agitated prior to the descent towards scission. Therefore one should expect an ever increasing degree of twisting as the impinging neutron energy is raised, an effect that might be observable.

The bending mode is somewhat intermediate and without a more precise estimate of t_{fiss} it is not possible to make specific predictions. But if scission occurs at $c = 2$ fm and t_{fiss} is several times 10^{-21} s, then the bending mode is expected to be agitated to an appreciable degree, though likely not fully. If bending is not fully agitated, wriggling will dominate and the fragment spins will tend to have parallel directions and their magnitudes will fluctuate in concert. The recent experimental results by Wilson *et al.* [4], suggesting that the spin magnitudes are in fact mutually fairly independent, puts a limit on the possible suppression of the bending mode. It would be very interesting to quantify this by further measurements.

Furthermore, because t_{bend} depends on the mass asymmetry, the degree of bending at scission should increase with the asymmetry. Because the fragment mass is a readily measurable fission observable, this feature is susceptible to experimental investigation as well.

On the basis on these estimates, we expect the wriggling modes to have reached full equilibrium at scission, while the bending modes may fall somewhat short of that, and though some twisting may be present it is not likely to play a major role.

Finally, TKE-gated data may also provide valuable information because small TKE values are associated with elongated scission configurations which take more time to reach. Consequently, if the bending mode is only partially equilibrated, it should have a larger presence in events with small TKE and a smaller presence in events with large TKE. This should be reflected, for example, in the degree of correlation between the two fragment spin magnitudes, something that should also be readily measurable.

IV. EVENT-BY-EVENT SIMULATION

The angular momentum treatment described above has been incorporated into the fission simulation code FREYA [26–28].

At the time of scission, each of the normal modes m is sampled from a Boltzmann distribution with an effective temperature $T_m = c_m T_{sc}$ where T_{sc} is the temperature of the dinuclear complex at scission and the coefficient c_m can be adjusted to allow exploration of different degrees of agitation. Thus the distribution of the mode amplitude s_m is $P(s_m) \sim \exp(-s_m^2/2\mathcal{I}_m T_m)$.

In our studies, we shall explore the sensitivity of the observables to the degree of agitation of the various rotational modes. For this purpose, it is convenient to characterize a particular physical scenario by the coefficients $(c_{\text{wrig}}, c_{\text{bend}}, c_{\text{twst}})$. The standard version of FREYA uses $(c_{\text{wrig}}, c_{\text{bend}}, c_{\text{twst}}) = (1, 1, 0)$, *i.e.* wriggling and bending are both fully agitated while there is no twisting [27, 28]. When other proportions are employed, the coefficients $\{c_m\}$ are renormalized to ensure that the fragment spin magnitudes remain unchanged on average.

After their formation at scission, the primary fission fragments separate along Coulomb trajectories, leading to two freely moving compound nuclei. The associated rotation of the dinuclear axis $\mathbf{R} \equiv \mathbf{R}_L - \mathbf{R}_H$ amounts to only a couple of degrees [27], so the free fragments are moving approximately along the direction of the fission axis. Subsequently, each fragment evaporates a number of neutrons, ν_L and ν_H , until its statistical excitation energy has fallen below the neutron separation energy, at which point the remaining excitation and rotation is disposed of by photon radiation.

We concentrate here on the photon radiation stage. For the purpose of the present study, FREYA has been modified relative to the standard version. Because of the (largely unknown) complexity of the fragments and their decays, we must employ a simplified description. The aim is to retain the essential features to a degree that makes it possible to bring out the physical effects we wish to discuss. If these turn out to be sufficiently promising to warrant experimental investigations, more refined treatments should be developed.

FREYA treats the neutron evaporation cascade in a classical manner, leaving the resulting product nucleus with a classical spin vector \mathbf{S} . The spin magnitude $S \equiv |\mathbf{S}|$ is now being replaced by a discrete value J that is either an integer or a half-integer according to whether the product mass number A is even or odd. Furthermore, it is assumed that the post-evaporation fragment is now in a quantum state that is maximally aligned along the spin direction $\hat{\mathbf{S}}$, so the initial state, before the photon radiation cascade, is given by $|i\rangle = |J, M=J\rangle$ when $\hat{\mathbf{S}}$ is used as the quantization axis.

In its ground state, the product nucleus may have an angular momentum directed along its symmetry axis; its magnitude is denoted by K_{gs} . The possible values of J are then $J = K_{\text{gs}}, K_{\text{gs}} + 1, \dots$ and the associated rota-

tional energy is

$$E_{\text{rot}} = \frac{J(J+1) - K_{\text{gs}}(K_{\text{gs}}+1)}{\mathcal{I}_{\perp}(A)}, \quad (10)$$

which vanishes in the ground state, $E_{\text{rot}}^{\text{gs}} = 0$. We use 50% of the rigid moment of inertia, $\mathcal{I}_{\perp}(A) = 0.5 \times \frac{2}{5} m A R_A^2$. The statistical excitation energy is then given by $E_{\text{stat}} = E_{\text{tot}} - E_{\text{rot}}$, where E_{tot} denotes the total excitation of the mother state.

As in the standard FREYA treatment, we assume that the nucleus first disposes of its statistical excitation energy through a sequence of E1 dipole photon emissions, continuing until the nucleus has reached the yrast line, *i.e.* the ground-state rotational band, along which there is no statistical excitation. For even-even nuclei, K_{gs} vanishes and the yrast states have even J values only, $J = 0, 2, 4, \dots$

The simulation of the E1 cascades is carried out with a recently developed semi-classical method [29] that replaces the generally complicated daughter state with a state that is also maximally aligned but along a direction that may be tilted relative to that of the mother state. This method is introduced elsewhere [29] and the details are not important for the present objective.

In this study, we concentrate on the sequential emission of collective E2 photons along the ground-state band in even-even product nuclei. Such emission processes are particularly simple, because when the mother state is maximally aligned, then so is the daughter state, and, importantly, the emission does not change the alignment direction of the nuclear spin, it only reduces its magnitude by $2\hbar$,

$$|J, J\rangle \rightarrow |J-2, J-2\rangle \rightarrow \dots \rightarrow |0, 0\rangle. \quad (11)$$

It follows that all the photons emitted in each collective cascade are mutually uncorrelated and they all have the same angular distribution.

The angular distribution of a photon emitted from a maximally aligned state $|J, J\rangle$ has a particularly simple form when expressed in polar coordinates (θ, ϕ) defined relative to the quantization axis (which we shall refer to as the spin direction). Generally, the distribution has azimuthal symmetry (*i.e.* it is symmetric around the spin direction and thus independent of ϕ). For a stretched E2 transition, the distribution of the polar angle is given by

$$P_{2,h}^2(\theta) = \frac{5}{2} (d_{2,h}^2(\theta))^2 = \frac{5}{8} (1 + h \cos \theta)^2 \sin^2 \theta, \quad (12)$$

where $d_{2,h}^2(\theta)$ is a Wigner d -function. It is important for the discussion in Sect. VI that the photon helicity $h = \pm 1$ enters in the angular distribution of each photon. The above distribution is normalized, $\int P_{2,h}^2(\theta) d \cos \theta = 1$.

V. ANGULAR DISTRIBUTION OF COLLECTIVE PHOTONS

It is experimentally possible to identify specific E2 transitions that stand out sufficiently clearly above the

background, a feature that can be used to identify the emitting product nucleus. To exploit this, we have selected a number of even-even product nuclei and henceforth focus on events that lead to those. The FREYA simulation treatment allows us to include all collective photons emitted in the course of the deexcitation of the selected product nuclei. While this would not be possible experimentally, because not all transitions in a given collective cascade can be identified, nor can all of the photons emitted in an event be detected, this practical challenge should not be prohibitive because the signal we seek receives additive contributions from each identified E2 transition at any stage of the collective cascade and from all even-even product nuclei. Therefore, for illustration, we present angular distributions averaged over all those collective transitions; this automatically takes account of the increased intensity of the lower transitions.

The key observable we discuss here is the angular distribution of the collective photons, measured relative to the direction of motion of the corresponding product emitter. Thus, photons emitted from the light product are measured relative to the direction of the light product, while photons emitted from the heavy product are measured relative to the direction of the heavy product. This may not be what would be done in an actual experiment in which typically only one of the two product nuclei is detected, but that complication matters little because the two fragments move very nearly oppositely and it is, by assumption, possible to tell which fragment any given E2 photon came from.

The utility of this observable lies in the fact that it is sensitive to the direction of the angular momentum of the emitting nucleus. For example, rather trivially (and unrealistically), if the fragment spin was directed along the direction of the fragment motion before the emission, then the resulting angular distribution of the emitted E2 photons, in terms of $\theta_{\gamma f}$, the angle between the emission direction and the velocity of the emitter nucleus, would be given by

$$W_{\parallel}(\theta_{\gamma f}) \sim 1 + hP_1(\cos\theta_{\gamma f}) - \frac{5}{7}P_2(\cos\theta_{\gamma f}) - hP_3(\cos\theta_{\gamma f}) - \frac{2}{7}P_4(\cos\theta_{\gamma f}), \quad (13)$$

as follows directly from Eq. (12).

However, a much more realistic (though still somewhat idealized) scenario is that the spin of the emitting nucleus is perpendicular to the motion of the fragment. In that case the basic angular distribution, which is given in Eq. (12) in terms of the angle between the photon motion and the emitter spin, $\theta_{\gamma S}$, must be averaged over all the equally likely perpendicular directions of \mathbf{S} . Generally, if the basic distribution is given by $dN/d\cos\theta_{\gamma S} = \sum_n \alpha_n P_n(\cos\theta_{\gamma S})$ then the directional average yields the distribution $dN/d\cos\theta_{\gamma f} = \sum_n \alpha'_n P_n(\cos\theta_{\gamma f})$ where the α'_n coefficients vanish for odd orders and the even ones are given by $\alpha'_{2n} = c_n \alpha_{2n}$ with (see the Appendix)

$$c_n = \frac{(-1)^n (2n)!}{2^{2n} (n!)^2} = 1, \frac{1}{2}, \frac{3}{8}, \frac{5}{16}, \dots \quad (14)$$

Thus the directional average removes the odd orders, and thereby also the helicity dependence, and the observable distribution in the perpendicular scenario becomes

$$W_{\perp}(\theta_{\gamma f}) \sim 1 + \frac{5}{14}P_2(\cos\theta_{\gamma f}) - \frac{3}{28}P_4(\cos\theta_{\gamma f}), \quad (15)$$

which differs qualitatively from the above distribution for the parallel scenario, Eq. (13).

As discussed in Sect. II, it is expected theoretically that the angular momenta of the primary fragments are nearly perpendicular to the dinuclear axis at the time of scission, $\hat{\mathbf{R}}(t_{\text{sciss}})$ and this is also what experiment suggests [14, 15], so the observed distribution may not differ very much from (15). However, even if the spins were originally perfectly perpendicular to $\hat{\mathbf{R}}(t_{\text{sciss}})$, they would not be perpendicular to the direction of the asymptotic fragment motion, not only because of the (slight) Coulomb rotation mentioned above but primarily because of the recoils from the evaporated neutrons and the preceding statistical (E1) photons.

Figure 2 shows the angular distribution $dN/d\cos\theta_{\gamma f}$ for different assumptions about the presence of the various dinuclear rotational modes, as obtained by specifying the parameters $\{c_m\}$ in the FREYA event-by-event simulation. As a useful reference, the idealized distributions $P_{\parallel}(\theta_{\gamma f})$ and $P_{\perp}(\theta_{\gamma f})$ are shown for each scenario.

All the distributions are well represented by a fourth-order Legendre fit,

$$dN/d\cos\theta \sim 1 + A_1 P_1(\cos\theta) + \dots + A_4 P_4(\cos\theta). \quad (16)$$

The calculated angular distribution coefficients $\{A_n\}$, averaged over all 22 product nuclei considered and over all stretched transitions up to $8 \rightarrow 6$, are shown in Table I. While the idealized distributions $P_{\parallel}(\theta_{\gamma f})$ and $P_{\perp}(\theta_{\gamma f})$ are symmetric around 90° , the simulated distributions are forward skewed due to the motion of the emitting fragment relative to the laboratory frame. For the relatively small fragment velocities occurring, it is a good approximation to correct for this focusing effect by retaining only the even Legendre terms.

The top panel (a) shows the standard FREYA scenario in which both wriggling and bending are fully present. Both of these modes contribute fragment spins that are perpendicular to the dinuclear axis and the symmetrized distribution is therefore close to $P_{\perp}(\theta_{\gamma f})$. The difference is due to the spin dealignment caused by prior emissions. These results are consistent with those obtained in the earlier experiments [14, 15]. [However, those data, which were taken over fifty years ago, have relatively large error bars and exhibit significant variations from nucleus to nucleus; some of the reported A_2 values are inconsistent with E2 transitions; the overall average of the values are $\langle A_2 \rangle_{\text{exp}} = 0.30 \pm 0.16$ and $\langle A_4 \rangle_{\text{exp}} = -0.07 \pm 0.21$.]

The second panel (b) shows a perhaps more realistic scenario in which bending is not fully agitated while twisting is somewhat agitated. The resulting angular distribution has become more isotropic but differs only slightly from the standard FREYA scenario in (a) and still

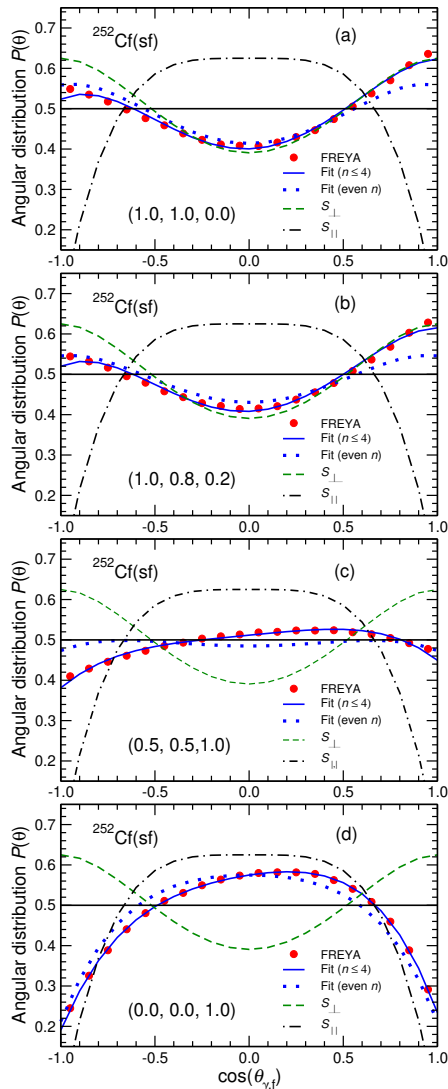


FIG. 2: The angular distribution of the collective E2 photons relative to the direction of the emitting product nucleus for four different scenarios: The standard FREYA scenario, in which the perpendicular modes (wriggling and bending) are fully agitated, while the parallel mode (twisting) is absent (a); a perhaps more realistic scenario in which bending is not fully agitated while twisting is somewhat agitated (b); a (probably less realistic) scenario in which the perpendicular and the parallel modes are equally agitated (c); and an extreme scenario in which only twisting is present (d). The specified values of $(c_{\text{wrig}}, c_{\text{bend}}, c_{\text{twst}})$ are indicated for each scenario. The Legendre fits (solid curves) and their symmetric parts (dots) are shown, as are the distributions for perfectly perpendicular or perfectly parallel emitter spins.

has a pronounced prolate appearance. This scenario is also consistent with the data in Refs. [14, 15].

A probably less realistic scenario in which the perpendicular and the parallel modes are equally agitated is shown in the third panel (c). The symmetrized angular distribution has now become nearly isotropic.

Finally, the bottom panel (d) shows the distribution

Scenario	A_1	A_2	A_3	A_4
perpendicular spin	0	0.357	0	-0.107
(1.0, 0.0, 0.0)	0.068	0.234	0.020	-0.088
(1.0, 1.0, 0.0)	0.070	0.236	0.019	-0.089
(0.0, 1.0, 0.0)	0.071	0.233	0.020	-0.081
(1.0, 0.8, 0.2)	0.075	0.187	0.017	-0.057
(0.5, 0.5, 1.0)	0.070	0.005	0.010	-0.040
(0.0, 0.0, 1.0)	0.091	-0.448	-0.045	-0.115
parallel spin	0	-0.714	0	-0.286

TABLE I: The average angular distribution coefficients $\{A_n\}$ for a variety of scenarios characterized by the indicated values of $(c_{\text{wrig}}, c_{\text{bend}}, c_{\text{twst}})$. Also shown are the values for the idealized scenarios when the spin of the emitting fragment is either perpendicular (top) or parallel (bottom) to its velocity.

for a (probably quite unrealistic) twisting-dominated scenario. As would be expected (see above), the angular distribution is now sideways peaked with an oblate form approaching that of the idealized distribution $P_{\parallel}(\theta_{\gamma, f})$.

The angular distribution coefficients $\{A_n\}$ are shown in Table I for a number of scenarios, including those shown in Fig. 2. The first three scenarios are purely perpendicular, but have different proportions of wriggling and bending. As expected, these all lead to similar angular distributions, bringing out the fact that $dN/d\cos\theta$ is not sensitive to $c_{\text{bend}}:c_{\text{wrig}}$ but only to the admixture of twisting.

A suitable observable for determining the degree of twisting may be the $W(0^\circ):W(90^\circ)$ yield ratio, the forward yield relative to the sideways yield. This is illustrated in Fig. 3 showing the yield ratio as a function of the relative presence of twisting, as measured by the suppression coefficient c_{twst} . There is a pronounced, nearly linear, decrease as c_{twst} is increased from zero to one and it is noteworthy that even the visually small change in $dN/d\cos\theta$ in Fig. 2 when going from no twisting (top panel in Fig. 2) to 20% twisting (second panel in Fig. 2) produces a significant decrease in the yield ratio. It is also important that the yield ratio, while quite sensitive to c_{twst} , is practically independent of the relative proportion of wriggling and bending: The results for three very different values of $c_{\text{bend}}:c_{\text{wrig}}$ are nearly identical.

VI. ANGULAR CORRELATIONS OF COLLECTIVE PHOTONS

We noted earlier that the angular distribution of the collective photons depends on the photon helicity $h=\pm 1$: Positive helicities tend to be associated with emission in the “northern” hemisphere, *i.e.* in the same direction as the spin of the mother nucleus, whereas photons with negative helicity are preferentially emitted into the “southern” hemisphere. This feature is intuitively ex-

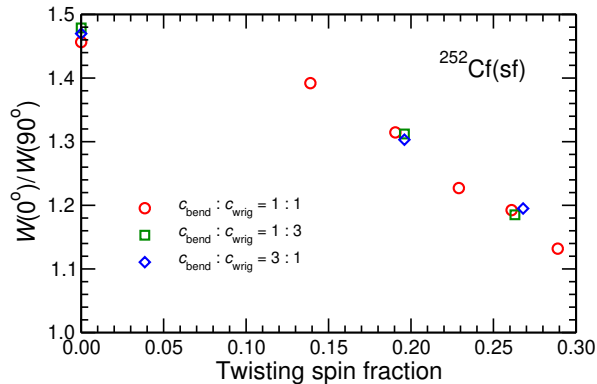


FIG. 3: The ratio of the photon yield in the direction of the fragment, $W(0^\circ)$, and the transverse yield, $W(90^\circ)$, as a function of the coefficient c_{twst} controlling the degree of agitation of the twisting mode, $T_{\text{twst}} = c_{\text{twst}} T_{\text{sc}}$.

pected: the photon tends to spin in the same sense as the emitting nucleus.

Consequently, the measurement of the helicities could provide information about the fragment spin direction. In particular, photon-photon correlation measurements could reveal information about the *relative* orientation of the spins of the two fragment partners.

As a quantitative illustration of this novel type of observable, we consider the distribution of the relative opening angle between two collective (E2) photons whose relative helicity is also being measured. (The term “relative” helicity refers to whether the two helicities are the same, $h_1 h_2 = +1$, or opposite, $h_1 h_2 = -1$.)

We concentrate on events leading to two even-even product nuclei for which (at least some of) the collective transitions can be experimentally identified and we then consider one such photon from each of the product partners. (The counting statistics can be improved significantly by utilizing the fact that all such photon pairs contribute additively to the observable.)

The opening angle between photon 1 and photon 2, ψ_{12} , is obtained from

$$\cos \psi_{12} = \cos \theta_1 \cos \theta_2 + \sin \theta_1 \sin \theta_2 \cos \phi_{12}, \quad (17)$$

where (θ_i, ϕ_i) is the direction of photon $i = 1, 2$ and $\phi_{12} = \phi_1 - \phi_2$ is the difference between their azimuthal angles. It is elementary to show that if the angular distributions of the individual photons are

$$dN_i/d\cos\theta_i = \sum_{n \geq 0} \alpha_n^{(i)} P_n(\cos\theta_i) \quad (18)$$

relative to a common axis, then the distribution of the opening angle is given by

$$P(\psi_{12}) = 2 \sum_{n \geq 0} \frac{\alpha_n^{(1)} \alpha_n^{(2)}}{2n+1} P_n(\cos\psi_{12}). \quad (19)$$

If only the positive perpendicular modes (wriggling) were populated at scission, the two fragment spins would

be perfectly parallel. Conversely, if only the negative perpendicular modes (bending) were populated at scission, the two fragment spins would be exactly opposite. If any subsequent realignment of the spins could be ignored, the corresponding individual angular distributions (*w.r.t.* the angle between the photon and the spin direction of the light product nucleus) would then be of the form (18) with the respective coefficients being

$$\alpha_0^{(i)} = \frac{1}{2}, \alpha_1^{(i)} = \pm \frac{1}{2} h_i \alpha_2^{(i)} = -\frac{5}{14}, \alpha_3^{(i)} = \mp \frac{1}{2} h_i \alpha_4^{(i)} = -\frac{1}{7}, \quad (20)$$

where upper signs refer to wriggling and lower signs refer to bending. The distribution of the opening angle between (any) two collective photons emitted from a pair of even-even product nuclei would therefore be

$$P^\pm(\psi_{12}) = \frac{1}{2} P_0(\cos\psi_{12}) \pm \frac{1}{6} h_1 h_2 P_1(\cos\psi_{12}) + \frac{5}{98} P_2(\cos\psi_{12}) \pm \frac{1}{14} h_1 h_2 P_3(\cos\psi_{12}) + \frac{2}{441} P_4(\cos\psi_{12}). \quad (21)$$

Thus the odd-order terms change signs when the fragment spins change from being parallel to being anti-parallel. Because the signs of these terms also depend on the helicities through their product $h_1 h_2$, those must be measured for the effect to be visible. (If the helicities were not detected, then the odd terms in $P(\psi)$ would average out.)

In order to examine the sensitivity of $P(\psi_{12})$ to the degree of agitation of the various dinuclear rotational modes, we have simulated a number of scenarios with FREYA. The results are illustrated in Fig. 4. (These results are obtained for photon pairs that have the same helicity; if the detected pairs have opposite helicity, then all the graphs are reflected around $\psi_{12} = 90^\circ$.)

In each panel, the dashed curves show the form of $P(\psi_{12})$ if the two emitting fragments had their spins either perfectly aligned or perfectly anti-aligned at the time of the emission of the detected photon, given in Eq. (21).

In the top panel (a) only wriggling is included so the two fragments are formed with perfectly parallel spins and each of them are subsequently subjected to (relatively small) changes due to recoils from any neutron and photon emissions prior to the emission of the detected photon. It is seen that the resulting opening-angle distribution is very close to the ideal form $P^+(\psi_{12})$, the most notable difference occurring at small opening angles, $\psi_{12} \approx 0^\circ$.

The second panel (b) shows the opposite extreme in which only bending is included, so the two fragments are formed with perfectly opposite spins. The resulting opening-angle distribution is then very close to the ideal form $P^-(\psi_{12})$, the most notable difference occurring at large opening angles, $\psi_{12} \approx 180^\circ$.

The third panel (c) demonstrates that a similar result would ensue if only the twisting mode were agitated at scission, because that would also render the two fragment spins exactly opposite.

The standard FREYA treatment includes wriggling and bending equally while excluding twisting. As discussed

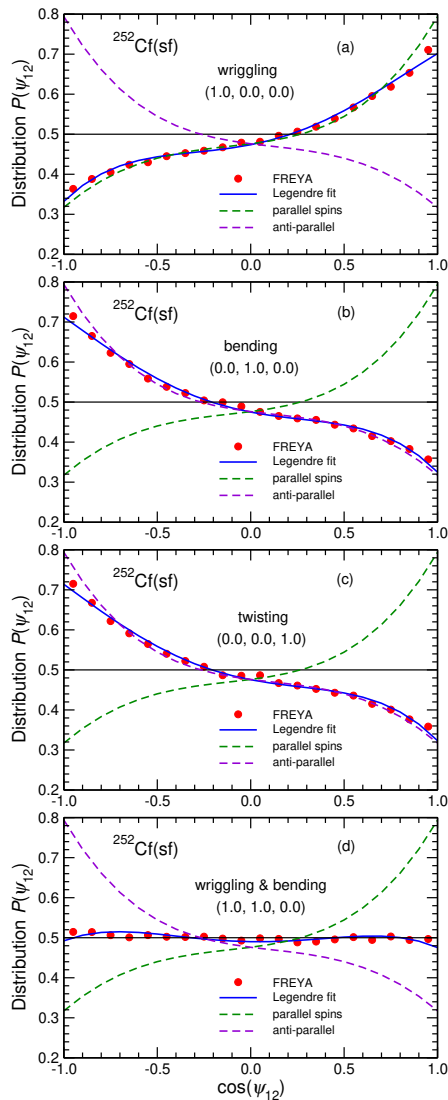


FIG. 4: The distribution of the opening angle ψ_{12} between pairs of E2 photons emitted from even-even product partners, for various scenarios for the dinuclear rotational modes at scission: Only wriggling is present (a); only bending is present (b); only twisting is present (c); and the standard FREYA scenario: wriggling and bending are equally present (d). Each panel shows the result of the FREYA simulations (dots) and the associated Legendre fit (solid curve), as well as the result of perfectly parallel or anti-parallel fragment spins at the time of emission. Only photon pairs with the same helicity are included; the results for photon pairs having opposite helicities would be reflected around $\psi_{12} = 90^\circ$.

recently [8], this leads to fragment spins that are very nearly uncorrelated. As a result, the opening angle ψ_{12} has a nearly constant distribution, as borne out in the bottom panel (d) of Fig. 4. This standard FREYA scenario is only a rough approximation to what would be theoretically expected (see Sect. II). A more realistic scenario would likely have somewhat less bending and somewhat more twisting, as considered in the second panel

(b) of Fig. 2. However, because the reduction of bending is largely compensated by the addition of twisting, this change in the relative presence of the various rotational modes has an almost negligible effect on $P(\psi_{12})$.

The above results suggest that helicity measurements would provide a powerful means for probing the relative direction of the angular momenta of fission fragment partners.

VII. CONCLUDING REMARKS

After formulating a convenient framework for the discussion of fission fragment angular momenta in terms of the normal modes of rotation in the dinuclear complex at scission, we invoked the Nucleon Exchange Transport model for the calculation of the relaxation times for those normal modes. By comparing these with estimates of the fission time, we concluded that wriggling should be sufficiently fast to be fully equilibrated at scission. The expected degree of bending increases with the mass asymmetry; while this mode is not expected to be fully agitated, its role may be larger for events with small fragment kinetic energies. Twisting is likely to play only a minor role, but it may grow more prominent as the excitation of the fissioning system is increased. These predicted features can be tested experimentally.

We then discussed how certain photon measurements may shed new light on the relative presence of the various rotational modes in fission. For this purpose, we here focussed on photons resulting from collective E2 transitions in even-even product nuclei which may be identified experimentally. These transitions preserve the spin orientation in the course of the collective photon cascade, so all the associated photons contribute additively to the observables discussed, greatly improving the statistics.

We particularly considered the angular distribution relative to the direction of a fission fragment, an observable that was first studied experimentally over fifty years ago [14, 15]. Using an appropriately refined version of the fission event generator FREYA, we simulated spontaneous fission of ^{252}Cf for a variety of scenarios with regard to the initial fragment spins, thus bringing out how sensitive the angular distribution is to the directionality of the fragment spins. We showed that the $W(0^\circ):W(90^\circ)$ yield ratio decreases steadily as the fragment spins become less perpendicular to the fission axis. The effect on this observable is approximately linear in the proportion of twisting and amounts to a decrease of $\approx 6\%$ for 20% twisting. We urge that such measurement be made, as our study indicates that sufficiently accurate data would provide quantitative information on the central issue of the direction of the fragment spins.

Finally, we discussed a novel observable, namely the distribution of the opening angle between pairs of helicity-tagged E2 photons emitted from even-even product partners. Contrary to the first observable, this one does not require the measurement of fragment directions.

However, it is essential to determine the photon helicities. Because this is beyond the current capabilities, our study serves to demonstrate the potential power of helicity measurements in connection with angular-momentum studies and to encourage the required technical developments. Based on our FREYA simulations, we demonstrated how the helicity-tagged opening-angle distribution is quite sensitive to the distribution of the opening angle between the initial angular momenta of the two fission fragment partners. This information has a crucial bearing on how the fragment spins are being generated at scission and thus such measurements would be invaluable for our understanding of this issue.

Acknowledgments

We wish to acknowledge helpful communications with B. Back, S. Marin, K.H. Schmidt, C. Schmitt, and J.B. Wilhelmy. This work was supported by the Office of Nuclear Physics in the U.S. Department of Energy's Office of Science under Contracts No. DE-AC52-07NA27344 (RV) and DE-AC02-05CH11231 (JR).

Appendix A: From $P(\theta_{\gamma S})$ to $P(\theta_{\gamma f})$

As discussed above, the angular distribution of the emitted photons relative to the spin direction of the emitting fragment can be written as

$$\frac{dN}{d\cos\theta_{\gamma S}} = \sum_{n \geq 0} \alpha_n P_n(\cos\theta_{\gamma S}), \quad (\text{A1})$$

where $\theta_{\gamma S}$ is the angle between the photon direction, $\hat{\omega}_\gamma = (\theta_{\gamma f}, \phi_{\gamma f})$, and the direction of the spin of the emitting fragment, $\hat{\omega}_S = (\theta_{Sf}, \phi_{Sf})$, where the polar direction is chosen along the fragment motion.

Because the azimuthal direction of the spin, ϕ_{Sf} , is undetermined, the observed angular distribution is obtained by averaging over ϕ_{Sf} . For that purpose, we invoke the Addition Theorem for spherical harmonics,

$$P_n(\cos\theta_{\gamma S}) = \frac{4\pi}{2n+1} \sum_{m=-n}^n Y_{nm}^*(\hat{\omega}_\gamma) Y_{nm}(\hat{\omega}_S), \quad (\text{A2})$$

where the spherical harmonics are given by

$$Y_{nm}(\hat{\omega}) = \left[\frac{2n+1}{4\pi} \frac{(n-m)!}{(n+m)!} \right]^{\frac{1}{2}} P_n^m(\cos\theta) e^{im\phi}. \quad (\text{A3})$$

Using $\int e^{im\phi} d\phi = 2\pi\delta_{m,0}$ and $P_n^0(x) = P_n(x)$, we can evaluate the azimuthal average of $P_n(\cos\theta_{\gamma S})$,

$$\int_0^{2\pi} \frac{d\phi_S}{2\pi} P_n(\cos\theta_{\gamma S}) = P_n(\cos\theta_{\gamma f}) P_n(\cos\theta_{Sf}), \quad (\text{A4})$$

and so the observed angular distribution becomes

$$\frac{dN}{d\cos\theta_{\gamma f}} = \sum_{n \geq 0} \alpha_n P_n(\cos\theta_{\gamma f}) P_n(\cos\theta_{Sf}). \quad (\text{A5})$$

In the special case when the fragment spin is perpendicular to the fragment motion, $\theta_{Sf} = \frac{1}{2}\pi$, we have $\cos\theta_{Sf} = 0$ so may use $P_{2n+1}(0) = 0$ and

$$P_{2n}(0) = \frac{(-1)^n}{\sqrt{\pi}} \frac{\Gamma(n + \frac{1}{2})}{\Gamma(n+1)} = \frac{(-1)^n (2n)!}{2^{2n} (n!)^2}, \quad (\text{A6})$$

leading to the relation used near Eq. (14),

$$\frac{dN}{d\cos\theta_{\gamma f}} = \sum_{n \geq 0} \frac{(-1)^n (2n)!}{2^{2n} (n!)^2} \alpha_{2n} P_{2n}(\cos\theta_{\gamma f}), \quad (\text{A7})$$

-
- [1] G.F. Bertsch, T. Kawano, and L.M. Robledo, Angular momentum of fission fragments, *Phys. Rev. C* **99**, 034603 (2019).
- [2] A. Al-Adili, Z. Gao, M. Lantz, A. Solders, M. Österlund, and S. Pomp, Isomer Yields in nuclear fission, *EPJ Web Conf.* **256**, 00002 (2021).
- [3] M. Travar et al., Experimental information on mass-and TKE-dependence of the prompt fission-ray multiplicity, *Phys. Lett. B* **817**, 136293 (2021).
- [4] J. Wilson *et al.*, Angular momentum generation in nuclear fission, *Nature (London)* **590**, 566 (2021).
- [5] R. Vogt and J. Randrup, Angular momentum effects in fission, *Phys. Rev. C* **103**, 014610 (2021).
- [6] A. Bulgac, I. Abdurrahman, S. Jin, K. Godbey, N. Schunck, and I. Stetcu, Fission Fragment Intrinsic Spins and Their Correlations, *Phys. Rev. Lett.* **126**, 142502 (2021).
- [7] P. Marević, N. Schunck, J. Randrup, and R. Vogt, Angular momentum of fission fragments from microscopic theory, *Phys. Rev. C* **104**, L021601 (2021).
- [8] J. Randrup and R. Vogt, Generation of fragment angular momentum in fission, *Phys. Rev. Lett.* **127**, 062502 (2021).
- [9] S. Marin, M.S. Okar, E.P. Sansevero, I.E. Hernandez, C.A. Ballard, R.L. Vogt, J. Randrup, P. Talou, A.E. Lovell, I. Stetcu, O. Serot, O. Litaize, A. Chebboubi, S.D. Clarke, V.A. Protopopescu, and S.A. Pozzi, Structure in the event-by-event neutron- γ multiplicity correlations in $^{252}\text{Cf}(\text{sf})$, *Phys. Rev. C* **104**, 024602 (2021).
- [10] I. Stetcu, A.E. Lovell, P. Talou, T. Kawano, S. Marin, S.A. Pozzi, and A. Bulgac, Angular momentum removal by neutron and γ -ray emissions during fission fragment decays, *Phys. Rev. Lett.* **127**, 222502 (2021).
- [11] A. Bulgac, I. Abdurrahman, K. Godbey, and I. Stetcu, Fragment Intrinsic Spins and Fragments' Relative Orbital Angular Momentum in Nuclear Fission, *Phys. Rev. Lett.* **128**, 022501 (2022).
- [12] S. Marin, E.P. Sansevero, M.S. Okar, I.E. Hernandez,

- S.D. Clarke, R. Vogt, J. Randrup, V.A. Protopopescu, and S.A. Pozzi, Directional-dependence of the event-by-event neutron- γ multiplicity correlations in $^{252}\text{Cf}(\text{sf})$, *Phys. Rev. C* **105**, 054609 (2022).
- [13] T. Wang, G. Li, L. Zhu, Q. Meng, L. Wang, H. Han, W. Zhang, H. Xia, L. Hou, R. Vogt, and J. Randrup, Correlations of neutron multiplicity and γ -ray multiplicity with fragment mass and total kinetic energy in spontaneous fission of ^{252}Cf , *Phys. Rev. C* **93**, 014606 (2016).
- [14] J. B. Wilhelmy, E. Cheifetz, R. C. Jared, S. G. Thompson, H. R. Bowman, and J. O. Rasmussen, Angular Momentum of Primary Products Formed in the Spontaneous Fission of ^{252}Cf , *Phys. Rev. C* **5**, 2041 (1972).
- [15] A. Wolf and E. Cheifetz, Angular distributions of specific gamma rays emitted in the deexcitation of prompt fission products of ^{252}Cf , *Phys. Rev. C* **13**, 1952 (1976).
- [16] J. R. Nix and W. J. Swiatecki, Studies in the liquid-drop theory of nuclear fission, *Nucl. Phys.* **71**, 1 (1963).
- [17] L. G. Moretto and R. P. Schmitt, Equilibrium statistical treatment of angular momenta associated with collective modes in fission and heavy-ion reactions, *Phys. Rev. C* **21**, 204 (1980).
- [18] T. Døssing and J. Randrup, Dynamical evolution of angular momentum in damped nuclear reactions: (I) Accumulation of angular momentum by nucleon transfer, *Nucl. Phys. A* **433**, 215 (1985).
- [19] J. Randrup, Theory of transfer-induced transport in nuclear collisions, *Nucl. Phys. A* **327**, 490 (1979).
- [20] J. Randrup, Transport of angular momentum in damped nuclear reactions, *Nucl. Phys. A* **383**, 468 (1983).
- [21] W.U. Schröder, J.R. Birkelund, J.R. Huizenga, W.W. Wilcke, and J. Randrup, Effect of Pauli Blocking on Exchange and Dissipation Mechanisms Operating in Heavy-Ion Reactions, *Phys. Rev. Lett.* **44**, 308 (1980).
- [22] W. U. Schröder and J. P. Huizenga, in *Treatise On Heavy-Ion Science*, edited by D.A. Bromley (Plenum, New York, 1984), p. 115.
- [23] J. Błocki, Y. Boneh, J.R. Nix, J. Randrup, M. Robel, A.J. Sierk, and W.J. Swiatecki, One-Body Dissipation and the Super-Viscosity of Nuclei, *Ann. Phys.* **113**, 330 (1978).
- [24] B.B. Back, Experimental measures of fission time scales, *Proceedings of the Sixth International Conference on Fission and Neutron-Rich Nuclei*, Sanibel Island, Florida, Nov. 6-12, 2016, Editor, J. Hamilton, World Scientific, Singapore (2017) p. 600.
- [25] B.B. Back, Experimental measures of fission time scales, *Proceedings of 13th International Conference on Nucleus-Nucleus Collisions*, JPS Conf. Proc. 32, 0100002 (2020).
- [26] J. M. Verbeke, J. Randrup, and R. Vogt, Fission Reaction Event Yield Algorithm, FREYA - For event-by-event simulation of fission, *Comp. Phys. Comm.* **191**, 178 (2015).
- [27] J. Randrup and R. Vogt, Refined treatment of angular momentum in FREYA, *Phys. Rev. C* **89**, 044601 (2014).
- [28] J. M. Verbeke, J. Randrup, and R. Vogt, Fission Reaction Event Yield Algorithm FREYA 2.0.2, *Comp. Phys. Comm.* **222**, 263 (2018).
- [29] J. Randrup and T. Døssing, Semi-classical simulation of γ cascades, in preparation.